MAIN ROTOR BLADE TIP VORTEX CHARACTERIZATION

Manuela Coletta, m.coletta@cira.it, Politecnico di Torino (Italy)
Fabrizio De Gregorio, f.degregorio@cira.it, CIRA (Italy)
Antonio Visingardi, a.visingardi@cira.it, CIRA (Italy)
Gaetano Iuso, gaetano.iuso@polito.it, Politecnico di Torino (Italy)

Abstract

The paper illustrates a research activity carried out at CIRA with the aim to characterize experimentally and numerically the blade tip vortices of a small scale four-bladed isolated rotor in hover flight and to evaluate their decay process during the convection of the wake downstream. 2C-2D PIV measurements were carried out below the rotor disk down to a distance of one radius. The numerical simulations were aimed at assessing the modelling capabilities and the accuracy of a free-wake Boundary Element Methodology. Several detection criteria were investigated in order to identify a suitable one for the analysis of PIV data. The Γ_2 vortex was selected as the most robust and reliable criterion and was applied to both experimental and numerical results. The tip vortices were characterised in terms of vorticity, circulation, swirl velocity, core radius and trajectory. The rotor wake mean velocity field and the instantaneous vortex characteristics were investigated. The experimental/numerical comparisons showed a reasonable agreement in the estimation of the mean velocity inside the rotor wake, whereas the BEM simulations predicted and under-estimated effect of the diffusion thus generating a smaller shear layer region with respect to the experiment. The numerical simulations provided a clear picture of the filament vortex trajectory interested by complex interaction starting at about a distance of z/R=-0.5. The time evolution of the tip vortices was investigated in terms of net circulation and swirl velocity. The PIV tip vortex characteristics showed a linear mild decay up to the region interested by vortex pairing and coalescence, where a sudden decrease, characterised by a large data scattering, occurred. The numerical modelling predicted a hyperbolic decay of the swirl velocity down to z/R=-0.4 followed by an almost constant decay. Instead, the calculated net circulation showed a gradual decrease throughout the whole wake development. The comparisons showed discrepancies in the region immediately downstream the rotor disk but significant similarities beyond z/R=-0.5.

1 NOMENCLATURE

Symbol	Description	Units
a_1	Squire's coefficient	
c	Chord length	m
D	Γ_2 domain radius	
r	Local radius	m
r_c	Vortex core radius	m
r_{c0}	Vortex core radius at $t = 0$	m
R	Rotor radius	m
t	Time	s
V_{Tip}	Blade tip speed ($= \Omega R$)	m/s
V_θ	Swirl (tangential) velocity	m/s
w	Downwash velocity	m/s
x, y, z	Geometrical coordinates	m
$\Delta x, \Delta y$	Space resolution	mm
α	Oseen constant	
Γ_0	Vortex circulation at $t = 0$	m^2/s
Γ_v	Vortex circulation	m^2/s
δ	Eddy viscosity coefficient	
ν	Kinematic viscosity	m^2/s
θ_0	Collective pitch angle	deg
σ	Rotor solidity	
ω	Out-of-PIV plane vorticity	$1/s$
ψ	Blade azimuth angle	deg
Ω	Rotor speed	RPM

2 INTRODUCTION

A low-budget research activity was carried out at CIRA in the framework of the GARTEUR Action Group 22 *Forces on Obstacles in Rotor Wake* (Visingardi et al.[1]) with the aim to numerically and experimentally evaluate the mutual effects between a small scale helicopter rotor in hover flight and a cylindrical load located at different positions below the rotor disk. The experimental investigations concentrated on the blade tip vortices far from the rotor disk and their characteristics were evaluated mainly in terms of vorticity, tangential velocity and core radius. The numerical simulations were performed with the main purpose to assess the modelling capabilities and the accuracy of a free-wake Boundary Element Methodology. The results

Presented at 45th European Rotorcraft Forum, Warsaw, Poland, 17-20 September, 2019

were illustrated in a paper of the 44th European Rotorcraft Forum 2018 (De Gregorio et al.[2]).

Following this activity, new investigations focussed on the blade tip vortex characteristics and the dissipation phenomena when moving away from the disk of the isolated rotor (i.e. without cylinder). Particular attention was dedicated to the vortex detection criterion adopted on the PIV data, and a Master of Science thesis was assigned to this end (Coletta[3]).

A vortex is an intuitive and easily identifiable flow structure, present in many natural phenomena and, as such, it is widely investigated in fluid mechanics. In spite of this, a universally accepted definition of vortex is still missing. A first possible definition was given by Lugt[4]: "a vortex is the rotating motion of a multitude of material particles around a common centre''. About ten years later, Robinson[5] stated that "a vortex exists when instantaneous streamlines mapped onto a plane normal to the vortex core exhibit a roughly circular or spiral pattern, when viewed from a reference frame moving with the centre of the vortex core". Although the definition of vortex remains quite ambiguous, several criteria have been developed over the years for the identification of vortices, as discussed by Chakraborty et al.[6] and Kolar[7].

The most widely used local methods for vortex identification are based on the analysis of the velocity gradient tensor $\boldsymbol{\nabla u}$ and its three invariants. Examples are: the Q criterion by Hunt et al.[8]; the Δ criterion introduced by Dallmann[9], Vollmers et al.[10], and Chong et al.[11]; λ_2 criterion by Jeong and Hussain [12], the maximum of the gradient tensor and the maximum of the circulation (Vollmers[13]). These local vortex-detection criteria are not always suitable for PIV data affected by noise and spurious vectors, thus resulting in high velocity gradients. A possible solution was offered by the Γ_2 criterion proposed by Graftieaux et al.[14] and successfully applied to complex dynamic stall measurements on highly separated flow by Mulleners and Raffel[15].

The present paper illustrates the results of these new numerical and experimental investigations. Section 3 describes the main characteristics of the four-bladed rotor rig and the PIV measurement system. A comparison among available vortex-identification criteria and the adopted Γ_2 one is illustrated in section 4; in particular, the assessment of the Γ_2 method is discussed showing a parametric study on single theoretical vortices for different levels of noise and making comparisons with the other typical methods. The numerical methodology is illustrated in section 5, whereas the numerical/experimental comparison of the results obtained is fully documented in section 6. The conclusions are finally reported in section 7.

3 EXPERIMENTAL SET UP

3.1 Rotor rig

A dedicated rotor test rig was developed based on an existing commercial radio-controlled helicopter model (Blade 450 3D RTF), but largely customized and modified for the scope of the experiment, Figure 1. A four-bladed rotor with collective and cyclic control replaced the original two-bladed rotor hub. The rotor presented four untwisted, rectangular blades with radius of $R = 0.36\,m$, root cut-out at 16% of the radius, chord length of $c = 0.0327\,m$ and a NACA0013 airfoil throughout the blade span, Figure 2. The resulting rotor solidity value was equal to $\sigma = 0.116$. The clockwise rotor maximum speed was $\Omega = 1780\,RPM$, and the collective pitch angle θ_0 varied from 1^0 to 11.3^0.

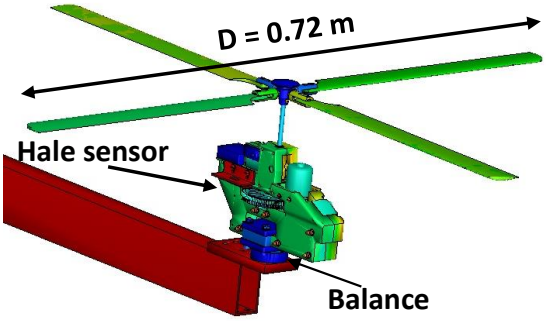

Figure 1: Rotor test rig

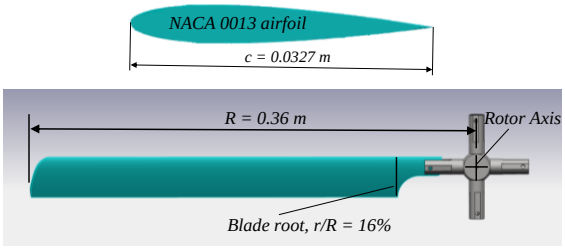

Figure 2: Airfoil (top) and planform (bottom) of the rotor blades, different scales in both sketches

3.2 PIV measurement system

The rotor downwash characteristics were measured by a standard two components measurement system composed by a double head Nd-Yag laser with a maximum energy of 320 mJ per pulse at 532 nm and a single double frame CCD camera (2048 by 2048 px). In order to track the blade tip vortices in the proximity to the rotor disk, measurement were performed using a 200 mm focal length obtaining a field of view of about 120 x 120 mm^2 and an optical resolution of about 17 px/mm. The time delay between the laser double–pulses was 25 μs.

The results presented a velocity spatial resolution of $\Delta x = 0.93\,mm$. The random noise of the PIV cross–correlation procedure can be estimated as 0.1 px as a rule–of–thumb. Using the current values for the optical resolution (17 px/mm) and the laser double–pulse delay (25 μs), this leads to a velocity error of ΔV of $\approx 0.23\,m/s$ for the PIV measurements. In the proximity to the rotor disk, the core radius r_c of the tip vortices was measured. The core radius is defined as the distance from the vortex centre to the radial position where the maximum swirl velocity is reached. Values of r_c between 3 and 3.3 mm were measured giving a ratio $\Delta x/r_c$ of about 0.31-0.28 comparable with the value of $\Delta x/r_c \leq 0.02$ indicated by Martin et al[16] in order to guarantee a correct vortex characterization.

Presented at 45th European Rotorcraft Forum, Warsaw, Poland, 17-20 September, 2019

4 VORTEX-IDENTIFICATION CRITERIA

The most widely used local methods for vortex identification are based on the analysis of the velocity-gradient tensor and its three invariants. In some cases, these local vortex-detection criteria are not suitable for PIV data, as for example in the regions affected by blade passage or the lower part of the rotor downwash where the tip vortex spirals are concentrated and the flow is highly turbulent. The possible solution is offered by the Γ_2 criteria proposed by Graftieaux et al [14]. The function Γ_2 is defined in discrete form as:

$$\Gamma_2(\vec{x_i}) = \frac{1}{M}\sum_{x_j \in S_i} \frac{\{(\vec{x_j} - \vec{x_i}) \times (\vec{u}_j - \vec{u}_{mean})\} \cdot \vec{n}}{|\vec{x_j} - \vec{x_i}||(\vec{u}_j - \vec{u}_{mean})|} \quad (1)$$

with S_i a two-dimensional circle around x_i with radius D, M the number of grid points x_j inside S_i with $j \neq i$, $\vec{n}$ the unit normal vector and u_j the velocity at x_j. According to its definition, Γ_2 is a 3D dimensionless scalar function, with $-1 \leq \Gamma_2 \leq 1$. The zones delimited by $|\Gamma_2| = \frac{2}{\pi}$ identify the vortices depicted by the measurement region. The vortex centre is identified as the maximum of the absolute of Γ_2 in the delimited zone. For each identified vortex, the centre position is measured and the main characteristics are calculated along the vortex radius in terms of swirl velocity, vorticity and circulation. The choice of the domain radius D has an influence on the dimension of the identified vortices and on the accuracy of the centre detection. In order to assess the reliability of the criteria, a parametric investigation was performed using a single or a pair of vortices (Coletta et al [17]). Vatistas vortices were investigated, eq.(2), varying the spatial resolution, the signal-to-noise level, the strength and the distance between each other in order assess the capacity of the criteria to discriminate each vortex. At the same time additional local vortex-identification criteria based on the velocity gradient were applied, in particular the Q criterion[8], the Δ criterion[9][10][11], the criterion of maximum vorticity[13] and the criterion of maximum circulation[13].

The isolated Vatistas vortex centre detection with and without noise is depicted in Figure 3. The data including noise were obtained by adding a white noise ranging between ±20% and ±90% of the value of the maximum tangential velocity, respectively.

The results shown in Figure 4 indicate that all methods are able to successfully detect the vortex centre in absence of noise or for a noise at ±20%, whereas only the Γ_2 criterion is not influenced by the random noise and is able to detect the vortex region and identify the vortex centre for the higher noise value (±90%). The positions of the detected centres are indicated by a red circle.

The occurrence of an incorrect vortex detection leads to a complete wrong measurement of the vortex characteristics, as shown in Figure 5 for the swirl velocity versus the rotor radius. A detailed description of the influence of the different parameters on the reliability of the Γ_2 criteria is given in Coletta et al.[17], where the spatial resolution and signal-to-noise ratio are also discussed in terms of optimal size of the domain radius D.

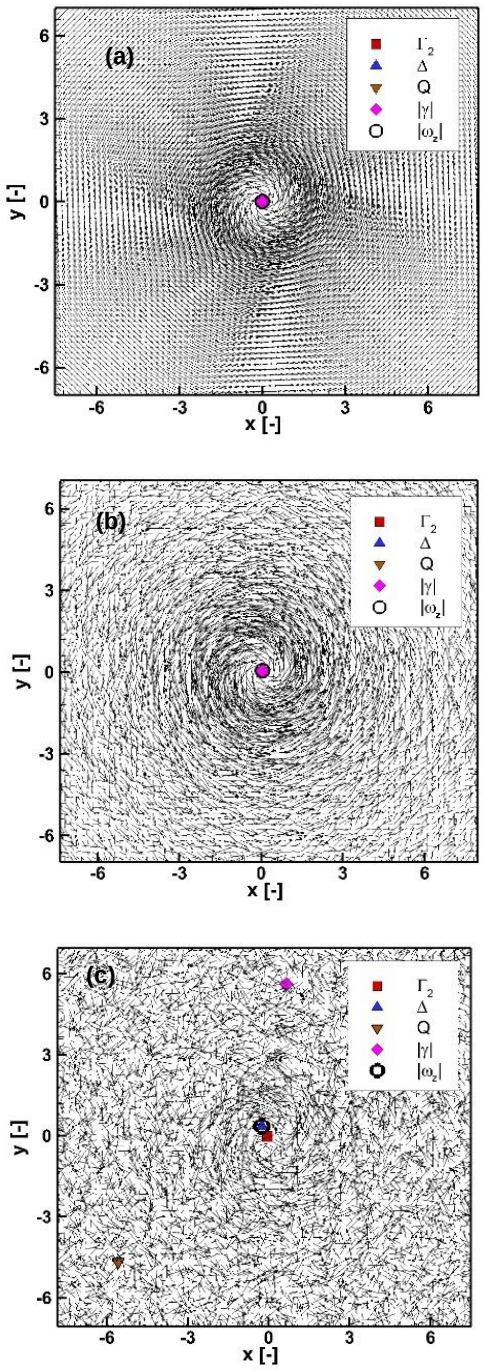

Figure 3: Vatistas vortex. Velocity field and centres with different methods. Noise 0% (a), noise 20% (b) and noise 90% (c).

Presented at 45th European Rotorcraft Forum, Warsaw, Poland, 17-20 September, 2019

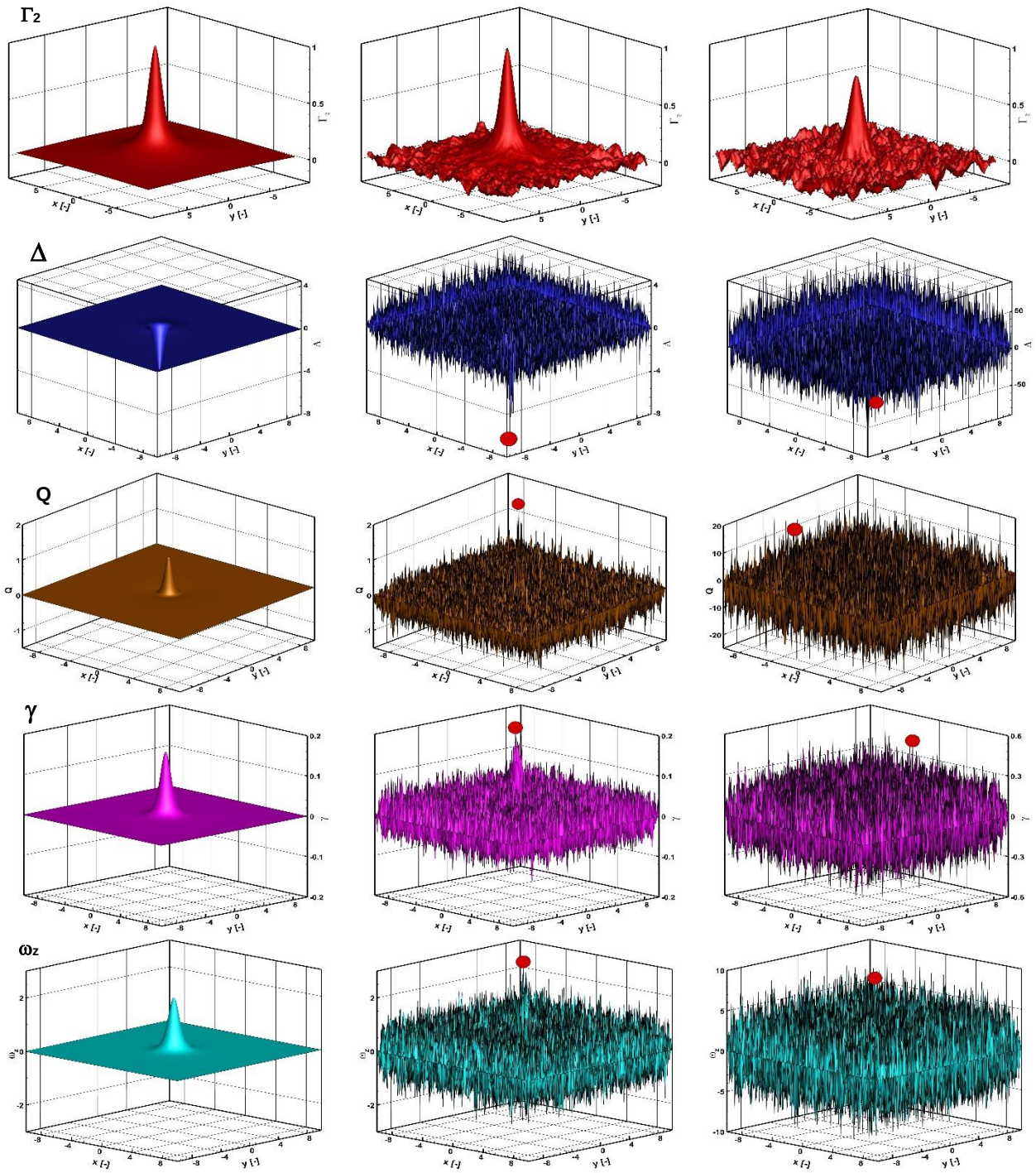

Figure 4: Vortex detection criteria applied to Vatistas vortex for different noise levels.

Presented at 45th European Rotorcraft Forum, Warsaw, Poland, 17-20 September, 2019

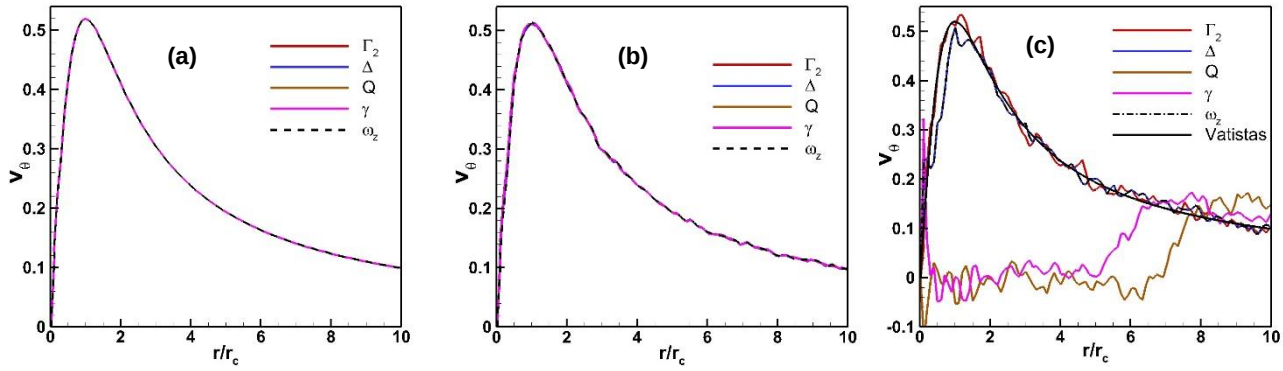

Figure 5: Vatistas vortex. Tangential velocity with different methods. Noise 0% (a), noise 20% (b), noise 90% (c)

5 NUMERICAL METHODOLOGY

5.1 BEM methodology

The numerical simulations were carried out by using the code RAMSYS[18], which is an unsteady, inviscid and incompressible free-wake vortex lattice boundary element methodology (BEM) solver for multi-rotor, multi-body configurations developed at CIRA. It is based on Morino's boundary integral formulation for the solution of Laplace's equation for the velocity potential φ. The surface pressure distributions are evaluated by applying the unsteady version of Bernoulli equation, which is then integrated to provide the forces and moments on the helicopter configuration and the surrounding obstacles.

In order to account for the viscous diffusion of the wake vortex elements, the Vatistas vortex core model was used, according to which the swirl velocity is expressed as:

$$V_\theta = \frac{r\Gamma_v}{2\pi(r^{2n} + r_c{}^{2n})^{1/n}} \quad (2)$$

where the coefficient n has been set equal to "1", as suggested by Scully[19].

The applied diffusion model is the one described by Squire[20]. In this model, the growth with time of the core radius r_c is given by:

$$r_c = \sqrt{r_{c0}^2 + 4\alpha\delta\nu t} \quad (3)$$

where the term r_{c0} is the initial core radius that removes the singularity at t_0, and was set equal to a 5% of the blade average chord length c in the calculations, the term α is the Oseen coefficient and is equal to 1.25643. The product $\delta\nu$ represents the "eddy viscosity" where ν is the kinematic viscosity and:

$$\delta = 1 + a_1 \frac{\Gamma_v}{\nu} \quad (4)$$

in which Γ_v is the circulation strength of the vortex element, while the Squire's coefficient a_1 is an empirical parameter specified to vary between 0.2 and 0.0002, as indicated in Bhagwat[21]. For a small-scale rotor, as the one used for these investigations, a value of $O(10^{-4})$ can be used.

The model suggested by Donaldson & Bilanin[22] was used to take into account the decay of the circulation Γ_v with time. According to this model, the circulation of the tip vortex $\Gamma_v(t)$ is expressed as:

$$\Gamma_v(t) = \Gamma_0 exp\left(-\frac{bq}{s}t\right) \quad (5)$$

being b a decay coefficient; q the ambient turbulence level and s the aircraft semispan. In the present calculations the coefficient bq/s was replaced with a single coefficient set equal to 2.5. This value was tuned, together with the empirical parameter a_1, finally set to 0.0003, in order to match several experimental observations[21],[23],[24] according to which the effective diffusion Squire/Lamb constant $\delta \approx 8$ for small scale helicopter rotors.

Figure 6 illustrates the decay of the normalized vortex circulation with the wake age obtained by applying the decay model of eq.(5) and using the value of 2.5 for the decay coefficient. Despite the slope is slightly lower than the measurements reported in Ramasamy et al.[23], a good agreement with the experimental results can be observed.

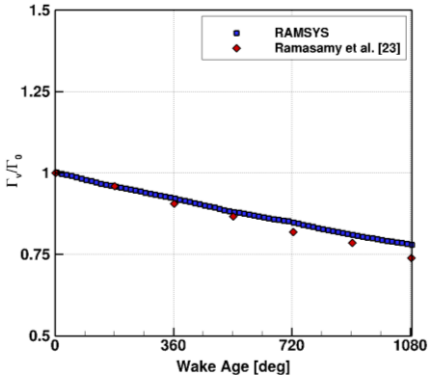

Figure 6: Normalized vortex circulation vs wake age.

Figure 7 shows the predicted growth of the vortex core radius as a function of wake age obtained by applying eq.(3) and using eq.(4) for the diffusion parameter δ and eq.(5) for the circulation decay. The picture highlights the close agreement of the calculated parameter δ with the constant value of 8, which is typical for small scale

Presented at 45th European Rotorcraft Forum, Warsaw, Poland, 17-20 September, 2019

helicopter rotors. The slight increasing deviation with the wake age from the value of 8 is produced by the application of the decay model in the vortex circulation.

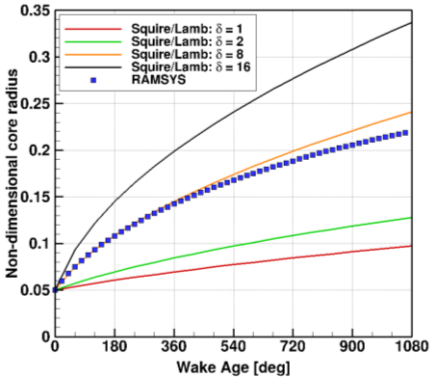

Figure 7: Growth of the vortex core radius as a function of wake age.

6 RESULTS

PIV measurements and BEM numerical simulations were carried out with the main purpose to investigate the structure and development of the rotor blade tip vortices.

6.1 Rotor wake ensemble-averaged flow field

The ensemble-averaged velocity field showed the shear layer region surrounding the rotor downwash wake.

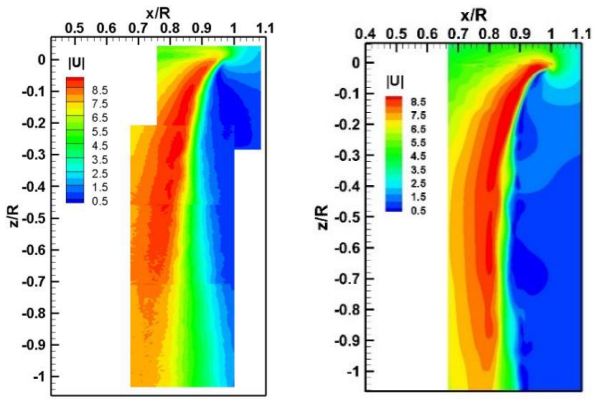

Figure 8: PIV (left) and numerical (right) ensemble average velocity magnitude colour map

The comparison between the experimental results, Figure 8-left, and the numerical predictions, Figure 8-right highlighted a general similarity but with two main differences:

a) in the experimental PIV the origin of the shear layer is identified at about x/R= 0.96 and slightly above z/R = 0 because of the deflection produced by the blade elasticity. Instead, the numerical results show the origin of the shear layer exactly at x/R=1 and z/R = 0, and this because the blade was modelled as a fully rigid body;

b) the diffusion produced by the viscous effects causes a marked thickening of the experimental shear layer moving downstream from the rotor disk, while the dissipation produces a reduction of the velocity magnitude which is already visible at around z/R=-0.7. These effects are less visible in the numerical results, despite diffusion and dissipation models were applied in the simulations.

A deeper investigation of the indicated differences was obtained by comparing the experimental and numerical z component of the induced velocity at several stations below the rotor disk in a region extending up to one radius below the rotor, Figure 9. The numerical results shown in the figure were evaluated at the several azimuthal stations of the last rotor revolution and time-averaged, whereas the velocity fluctuations, due to the flow field unsteadiness, was evaluated and represented in terms of RMS bars. The experimental PIV measurements were made in a fixed vertical plane during about 1500 rotor revolutions. The values were then ensemble-averaged and the velocity fluctuations were represented in terms of RMS bars.

The numerical predictions show a satisfactory agreement with the experiment in the radial region of the blade included from the root cut-out (16%) to the position $r/R = 80\%$, where the maximum of the inflow is measured. In the radial region, where the tip vortex roll up produces its greater effect, the numerical results show an upwash that is not present in the experiment. Furthermore, discrepancies between the numerical results and the experiment can also be observed in the region of the rotor hub, not modelled in the numerical simulations.

Finally, the different slope of the derivative $\partial w/\partial x$ between the experiment and the numerical simulation around 80%-100% of the blade radius was further analysed by comparing the PIV measurements made with a finer resolution ($\Delta x = 0.93\, mm$), with those at a resolution of ($\Delta x = 2.7\, mm$) and with the numerical results evaluated on a grid having a resolution of $\Delta x = \Delta z = 0.6\, mm$. The results showed that the slope evaluated by the finer PIV measurements are much closer to the numerical results but this happens until the z/R = 0.4. More downstream, the slope of the finer and coarser PIVs is about the same.

Presented at 45th European Rotorcraft Forum, Warsaw, Poland, 17-20 September, 2019

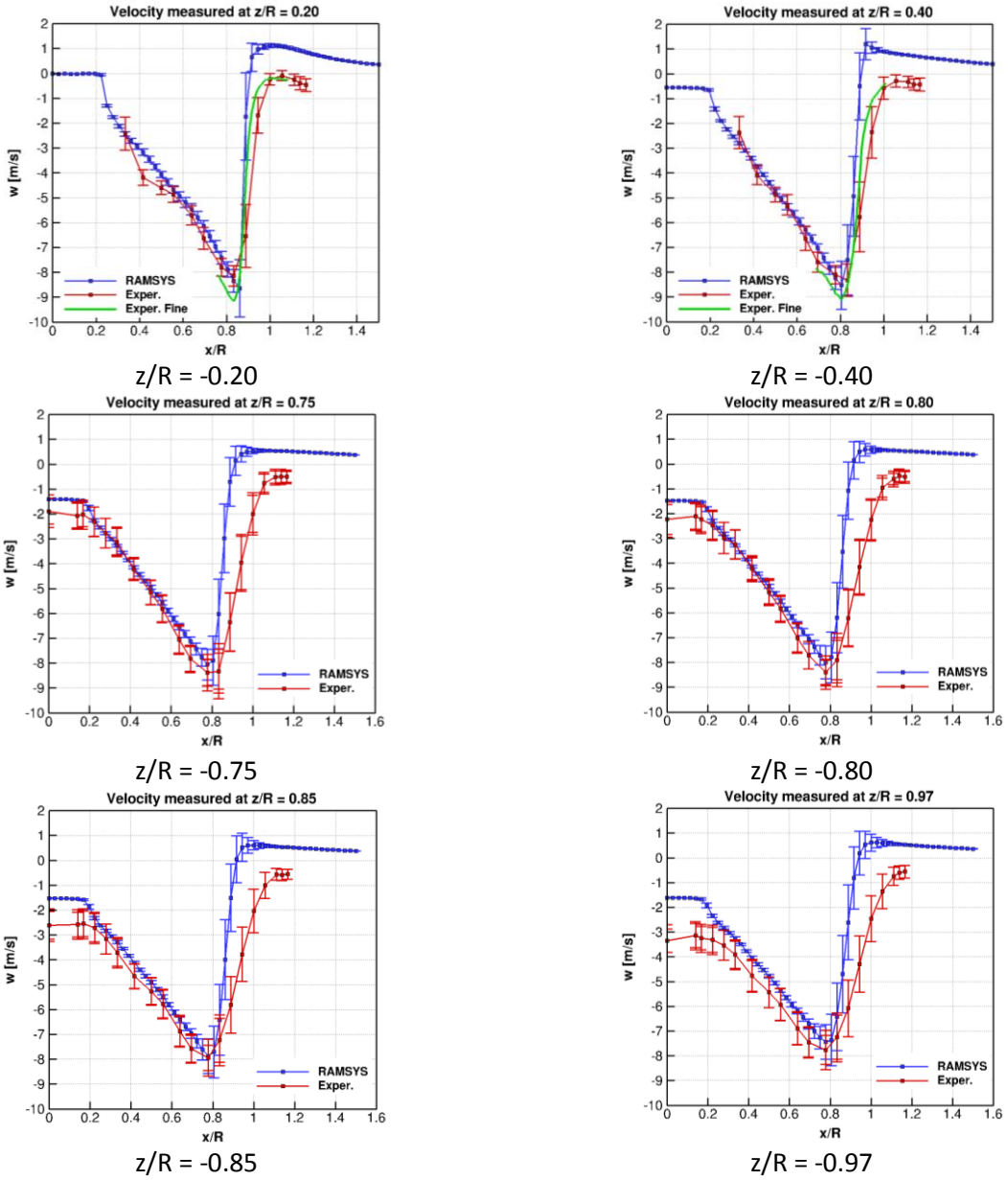

Figure 9: PIV vs numerical vertical velocity comparison.

6.2 Blade tip vortices

The application of the Γ_2 method to the PIV and BEM instantaneous velocity fields highlighted the presence of several tip vortices in the proximity to the blade, Figure 10. The PIV measurements were not phase locked with the rotor so that the age of the vortices was estimated on the basis of the position of the tip vortices with respect to the tip blade. In addition, three PIV tip vortices can be counted in the measurement region of the figure instead of the four predicted by the BEM simulation. This results in larger distances between consecutive PIV vortices with respect to the numerical ones.

Once the centres of the tip vortices were detected, the non-dimensional tangential velocities and circulations were calculated and represented versus the non-dimensional vortex radius. The characteristics of the BEM tip vortices were evaluated at a wake age of $\psi = 10°$, while the closest PIV tip vortices were selected by the analysis of more than 300 velocity fields.

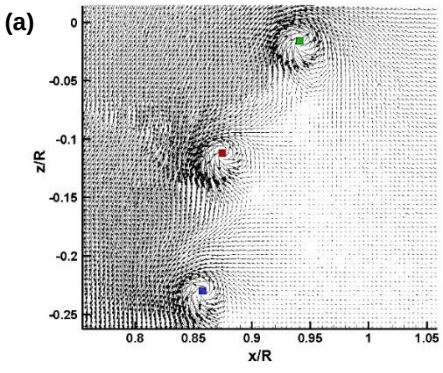

Presented at 45th European Rotorcraft Forum, Warsaw, Poland, 17-20 September, 2019

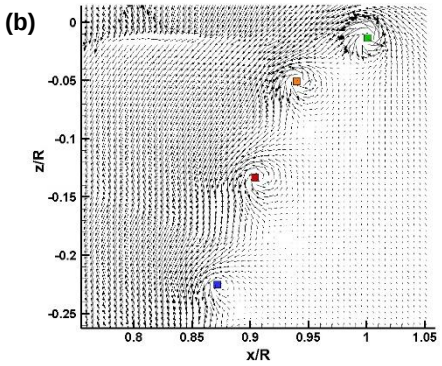

Figure 10: Comparison between PIV (a) and numerical (b) tip vortex locations with Γ_2 method

The results shown in Figure 11 provide the BEM/experimental comparisons for a set of vortices located at about the same distances from the rotor disk. The characteristics of the BEM vortices strictly follow the variation of the tangential velocity, circulation and vortex core radius as dictated by eq.(2), eq.(5) and eq.(3), respectively. The decrement of the BEM swirl velocity peak follows a hyperbolical trend, whereas in the PIV vortices it decreases almost linearly as the distance from the rotor disk increases. This turns out in a larger dissipation of the BEM vortices, if compared to the PIV ones, thus resulting in a smaller intensity of the BEM velocity peak with exception for the first vortex. Both BEM and PIV circulations decrease as the distance from the disk increases with the PIV, showing a vortex strength always larger than the numerical results. Similar trend and values are shown by the radius core behaviour for both data.

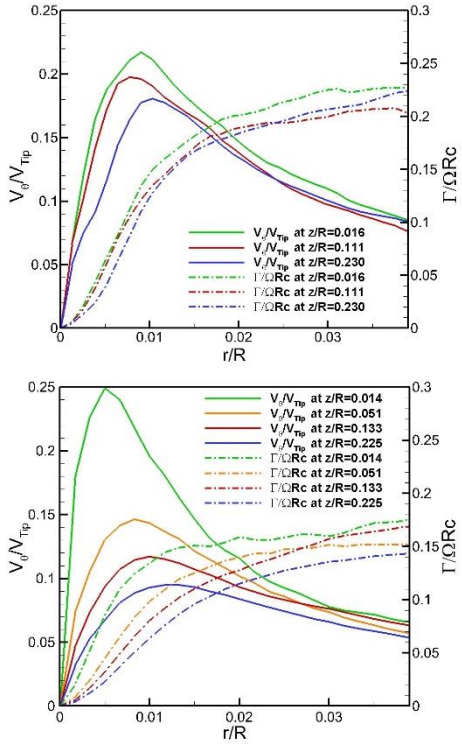

Figure 11: Tangential velocity and circulation for each vortex. PIV velocity (top), BEM velocity (bottom)

The distribution of the experimental vortex centres, Figure 12, showed the highest concentration in the proximity to the rotor disk and that their location was enclosed in the shear layer region. Moving downstream, the data scattering increased distributing the centres of the vortical structures both outside and inside the ensemble-averaged downwash, whereas the concentration of vortex decreased due to the fading and/or merging of vortices. The same representation for the numerical vortex centres showed an extremely narrow region of the shear layer and an almost full match between the boundaries of the shear layer region and the path of the vortex centres.

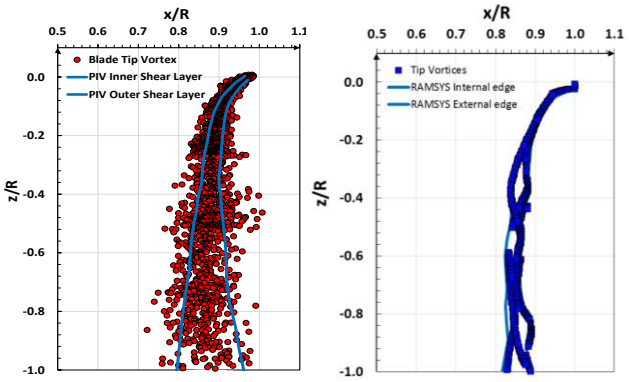

Figure 12: PIV (left) and numerical (right) position of blade tip vortices with respect to the shear layer region

An additional characterization of the instantaneous tip vortices was obtained by evaluating the component of the vorticity orthogonal to the PIV plane $\omega = (\nabla \times V)_{\perp}$ and comparing the experimental results with the numerical simulations.

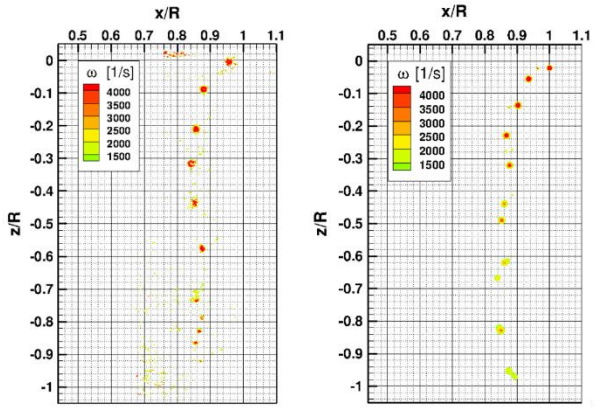

Figure 13: Experimental (left) and numerical (right) vorticity = $(\nabla \times V)_{\perp}$ in the PIV plane

Figure 13 illustrates the results of this comparison. A cut-off of the vorticity module was set at 1500 $1/s$ in order to remove as much as possible the flow field small-scale turbulence and to have a more concentrated representation of the tip vortices. PIV results generally show a stronger vorticity. The blade flexibility in the experiment generates the tip vortex at a higher and more inboard position with respect to the BEM result ($x/R \approx 0.96$; $z/R \approx 0$ vs $x/R \approx 1$; $z/R \approx -0.02$). The presence of widespread vorticity along the blade span around x/R=0.8 and z/R=0 can be observed in the PIV due to the blade passage.

Presented at 45th European Rotorcraft Forum, Warsaw, Poland, 17-20 September, 2019

The numerical simulations allowed the visualization of the entire wake structure generated by the rotor. In particular, it was possible to visualize the tip vortices and to associate them to the generating blades. Figure 14 shows the numerical tip vortex structure up to a distance of z=-1.5R below the rotor disk. Each of the four colours corresponds to a vortex filament generated by the relative blade. The image illustrates that the vortex structure keeps a geometrical regularity until a distance between z/R=-0.5 and -0.6, after which the wake starts showing a more chaotic behaviour. A second aspect that is highlighted in the figure is the pairing phenomenon according to which the mutual positions of the vortex filaments tend to interchange after a first rotor revolution. More specifically, looking at the sequence of the tip vortices at about x/R = +1.0, it is: cyan-blue-green-red during the first revolution, but becomes cyan-green-blue-red during the second revolution. This means that the vortices blue and green begin to roll up with each other until when they have completely interchanged their position after one revolution. Analogously, a similar behaviour can be observed at about x/R = -1.0, for the vortex filaments red and cyan. This mechanism contributes to increase the flow turbulence since from the third revolution onward.

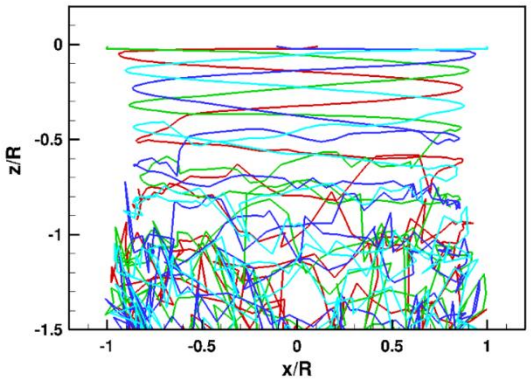

Figure 14: Blade tip vortices

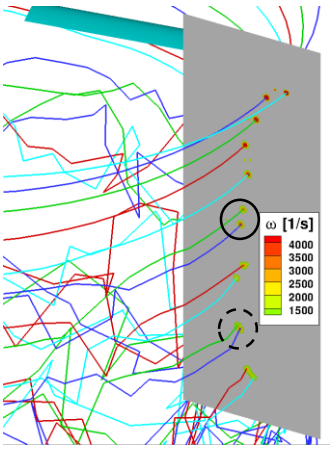

Figure 15: Numerical vorticity in the PIV plane and association with the generator vortex filaments

Figure 15 shows the association between the numerical vortex filaments and the generated vorticity in the plane corresponding to the PIV measurements. The pairing phenomenon is clearly visible after the second revolution between the green and blue vortex filaments, highlighted in figure by the black circle, with the vorticity intensity of the first one being smaller than that of the second one. The dashed black circle shows that during the third revolution the green and blue vortex filaments tend to coalesce.

Figure 16 shows a comparison between the experiment and the numerical simulation in terms of the variation of the non-dimensional net circulation of all the identified tip vortices versus the distance from the rotor disk z/R. The net circulation was determined at a distance of 0.25c from the vortex centre, and by assuming flow axisymmetry in the reference system moving with the vortex core, following the specification in Ramasamy et al.[23]. In the wake region between the rotor disk and where the pairing phenomenon occurs (z/R=-0.5), the experimental/numerical comparison shows a reasonable agreement in terms of negative slope, while an intensity difference of about 17% arises. Further downstream, the experimental slope first suddenly decreases and then realigns to the numerical trend but with smaller values.

The change in slope of the experimental data at z/R=-0.5 and their subsequent scattering at distances z/R < -0.5 might be explained by an increase in dissipation due to the growing of turbulence and by the process of pairing and coalescence of vortex filaments, respectively. This process was also mentioned in the explanation of the BEM tip vortices path of Figure 14. The numerical results resemble the trends illustrated in Figure 6. The merging of co-rotating vortices, which produce a higher circulation, likely causes the presence of higher values in the region $z/R \in [-0.8; -1.0]$.

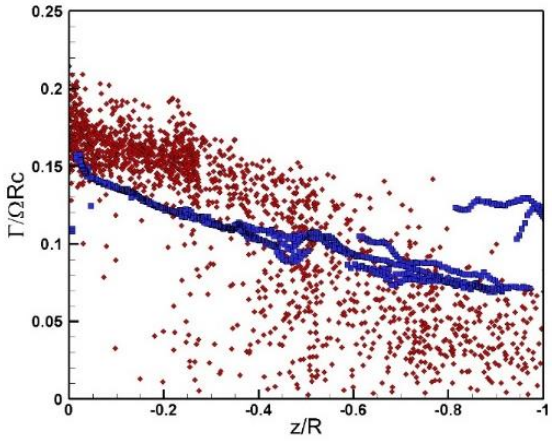

Figure 16: Non-dimensional net circulation. Comparison between the experiment (red diamond) and the numerical simulation (blue square)

Finally, Figure 17 shows a comparison between the experiment and the numerical simulation in terms of non-dimensional velocity swirl of all the identified tip vortices versus the distance z/R. The experimental vortices show a net difference in terms of slope and intensity before and after z/R = -0.5. The reason for this behaviour has the same explanation as for the net circulation trend discussed in Figure 16. The numerical results show a typical hyperbolical decay of the velocity intensity according to the model of eq.(2) combined with eq.(3). An interesting match with the

Presented at 45th European Rotorcraft Forum, Warsaw, Poland, 17-20 September, 2019

experiment can be observed for distances from the rotor disk lower than z/R = -0.5. The presence of higher values in the region z/R ∈ [-0.8; -1.0] is likely caused by the merging of co-rotating vortices which produce a higher velocity swirl, as also mentioned for the net circulation.

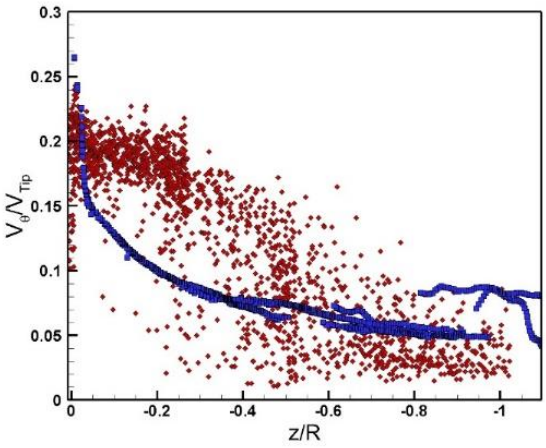

Figure 17: Non-dimensional velocity swirl. Comparison between the experiment (red diamond) and the numerical simulation (blue square)

7 CONCLUSIONS

A research activity was carried out at CIRA with the aim to characterize experimentally and numerically the blade tip vortices of a small scale four-bladed isolated rotor in hover flight and to evaluate their decay process during the convection of the wake downstream. 2C-2D PIV measurements were carried out below the rotor disk down to a distance of one radius. The numerical simulations were aimed at assessing the modelling capabilities and the accuracy of a free-wake Boundary Element Methodology.

The Γ_2 vortex centre detection criterion was applied both to the experimental and numerical results. A parametric investigation was performed using a Vatistas vortex model with the aim to assess the capability of the criteria to detect the centre. The spatial resolution, the signal-to-noise level and the strength were varied for the purpose. Once detected the centres, tip vortices were characterised in terms of vorticity, circulation, swirl velocity, core radius and trajectory.

The rotor wake mean velocity field and the instantaneous vortex characteristics were investigated. The experimental/numerical comparisons showed a reasonable agreement in the estimation of the mean velocity inside the rotor wake, whereas the BEM simulations predicted and under-estimated effect of the diffusion thus generating a smaller shear layer region with respect to the experiment.

The numerical results provide a clear picture of the filament vortex trajectory interested by complex interaction starting at about a distance of z/R=-0.5.

The time evolution of the tip vortices was investigated in terms of net circulation and swirl velocity. The PIV results showed a similar behaviour for both quantities. They showed a linear mild decay up to the region interested by vortex pairing and coalescence, where a sudden decrease, characterised by a large data scattering, occurred. The numerical modelling predicted a hyperbolic decay of the swirl velocity down to z/R=-0.4 followed by an almost constant decay. Conversely, the calculated net circulation showed a gradual decrease throughout the whole wake development.

The comparisons showed discrepancies in the region immediately downstream the rotor disk but significant similarities beyond z/R=-0.5.

The future activities will deal with:

- Time resolved PIV measurement shall be carried out in order to allow a direct comparison with the time history of numerical vortices;
- Implementation and testing of more sophisticated vortex decay models;
- Implementation of a model to take into account the vortex strain;
- Comparison with higher fidelity CFD simulations.

8 REFERENCES

[1] Visingardi, A., De Gregorio, F., Schwarz, T., Schmid, M., Bakker, R., Voutsinas, S., Gallas, Q., Boisard, R., Gibertini, G., Zagaglia, D., Barakos, G., Green, R., Chirico, G., Giuni, M., "Forces on Obstacles in Rotor Wake – A GARTEUR Action Group," 43rd European Rotorcraft Forum proceedings, Milan, Italy, September 12-15;

[2] De Gregorio, F., Visingardi, A., Nargi, R.E., "Investigation of a Helicopter Model Rotor Wake interacting with a Cylindrical Sling Load," proceedings of 44th European Rotorcraft Forum, Delft, The Netherlands, September 18-21, 2018;

[3] Coletta, M., "Identificazione di strutture vorticose nella scia di un rotore," MSc thesis, to be discussed in 2019;

[4] Lugt, H.J., "Vortex Flow in Nature and Technology," Wiley, 1983;

[5] Robinson, S.K., "Coherent motion in turbulent boundary layer," Annual Review of Fluid Mechanics, 23:601–639, 1991;

[6] Chakraborty, P., Balachandar, S., Adrian, R.J., "On the relationships between local vortex identification schemes," J. Fluid Mech., 535, 189–214, 2005;

[7] Kolar, V., "Vortex identification: New requirements and limitation," Journal of Heat and Fluid Flow, 28, 638-652, 2007;

[8] Hunt, J.C.R., Wray, A.A., Moin, P., "Eddies, stream, and convergence zones in turbulent flows," Center for Turbulence Research Report CTR-S88, pp. 193–208, 1988;

[9] Dallmann, U., "Topological structures of three-dimensional flow separation," DFVLR-IB Report No. 221-82A07, 1983;

[10] Vollmers, H., Kreplin, H.-P., Meier, H.U., "Separation and vertical type flow around a prolate spheroid – Evaluation of relevant parameters," in: Proc. of the AGARD Symposium on Aerodynamics of Vortical Type

Presented at 45th European Rotorcraft Forum, Warsaw, Poland, 17-20 September, 2019

Flows in Three Dimensions, Rotterdam, AGARDCP-342, pp. 14-1–14-14, 1983;

[11] Chong, M.S., “A general classification of three-dimensional flow fields,” Phys. Fluids A2, 765-777, 1990;

[12] Jeong, J., Hussain, F., “On the identification of a vortex,” J. Fluid Mech. 285, 69–94, 1995;

[13] Vollmers, H., “Detection of vortices and quantitative evaluation of their main parameters from experimental velocity data,” Meas. Sci. Technol. 12, 1199-1207, 2001;

[14] Graftieaux, L., Michard, M., Grosjean, N., “Combining PIV, POD and vortex identification algorithms for the study of unsteady turbulent swirling flows,” Meas. Sci. Technol. 12 1422–1429, 2001;

[15] Mulleners, K., Raffel, M, “The onset of dynamic stall revisited,” Exp Fluids doi:10.1007/s00348-011-1118-y, 2011;

[16] Martin, P.B., Pugliese, G.J., Leishman, J.G., Anderson, S.L., “Stereo PIV measurement in the wake of a hovering rotor,” presented at the 56th AHS Annual Forum, Virginia Beach, VA, USA, 2000;

[17] Coletta, M., De Gregorio F., Visingardi A., Iuso G., “PIV Data: Vortex Detection and Characterization,” 13th Internation Symposium on Particle Image Velocimetry, Munich, Germany, 2019;

[18] Visingardi, A., D'Alascio, A., Pagano, A., Renzoni, P., “Validation of CIRA's Rotorcraft Aerodynamic Modelling SYStem with DNW Experimental Data,” 22nd European Rotorcraft Forum, Brighton, UK, 1996;

[19] Scully, M.P., “Computation of Helicopter Rotor Wake Geometry and Its Influence on Rotor Harmonic Airloads,” MIT Aeroelastic and Structures Research Laboratory, ASRL TR 178-1, 1975;

[20] Squire, H.B., “The Growth of a Vortex in Turbulent Flow,” The Aeronautical Quarterly, 16: p. 302-306, 1965;

[21] Bhagwat, M.J., Leishman, J.G., “Generalized Viscous Vortex Model for Application to Free-Vortex Wake and Aeroacoustic Calculations,” presented at the 58th AHS Annual Forum, Montreal, Canada, June 11-13, 2002;

[22] Donaldson, C. duP., Bilanin, A.J., “Vortex Wakes of Conventional Aircraft,” AGARDograph, N.204, May 1975;

[23] Ramasamy, M., Leishman, J.G., “The Interdependence of Straining and Viscous Diffusion Effects on Vorticity in Rotor Flow Fields; presented at the 59th AHS Annual Forum, Phoenix (AZ), USA, May 6-8, 2003;

[24] Ramasamy, M., Leishman, J.G., “Reynolds Number Based Blade Tip Vortex Model,” presented at the 61st AHS Annual Forum, Gravepine (TX), USA, June 1-3, 2005

Presented at 45th European Rotorcraft Forum, Warsaw, Poland, 17-20 September, 2019